# Wearable alcohol monitoring device with auto-calibration ability for high chemical specificity

**Conference Paper** · June 2016

DOI: 10.1109/BSN.2016.7516287



**6 authors**, including:

Yogeswaran Umasankar
Florida International University
**76** PUBLICATIONS **1,652** CITATIONS

SEE PROFILE

Shekhar Bhansali
Florida International University
**211** PUBLICATIONS **4,078** CITATIONS

SEE PROFILE

# Wearable alcohol monitoring device with auto-calibration ability for high chemical specificity

Yogeswaran Umasankar, Ahmed H. Jalal, Pablo J. Gonzalez, Mustahsin Chowdhury, Alejandro Alfonso, Shekhar Bhansali*, *Florida International University, Miami, Florida 33174, United States*

*Abstract*— **Multimodal electrochemical method comprising open circuit potential and amperometric technique has been implemented to improve the specificity of the ethanol detection in a fuel cell sensor system. A miniaturized device with LMP91000 potentiostat and a processing unit has been constructed containing simple auto-calibration algorithm. The developed processing unit consist of a low power microcontroller (MSP430F5529LP). The sensing unit composed of a three electrode proton exchange membrane (PEM) fuel cell sensor, where Nafion is the PEM. In these studies, the signal due to interference has been eliminated with the support of algorithm and multimodal electrochemical method. The results show that the sensor can detect ethanol as low as 5ppm. The constructed device was validated by comparing it with the commercially available potentiostat, and the response was similar in both devices.**

## I. Introduction

A continuous alcohol measurement in a wearable platform is necessary to avoid various clinical and safety issues [1-4]. Breath alcohol devices are popular among law enforcement agencies for random monitoring of the driving under influence offenders [5-10]. Although, a random monitoring cannot cover the mass extent of the population. Further, the alcohol content in the blood will be excreted in about 8 hours. The offender can use this time window to get intoxicated and sober before next breath sampling. Contrarily, alcohol detection from skin perspiration replacing all other technologies owing to them in-situ, continuous and reliable blood alcohol content (BAC) monitoring [11]. The first prototype of transdermal alcohol monitoring device was an electrochemical cell, Giner WrisTAS, which relied on the current measurement technique. The major drawbacks of this device were, it could not resist water immersion and has no data acquisition system. The transdermal alcohol monitoring systems, such as secure continuous remote alcohol monitoring system, transdermal alcohol detection system, or CAM patrol plus has overcome these issues [12]. But they affected by false positive readings by environmental alcohol, tampering issues, slow response time, large size, needs frequent manual calibration, high operational costs and water accumulation, which made these systems ineffective.

In this work, a complete wearable platform has been developed capable of providing a comprehensive low power, high accuracy and easily sustainable electrochemical sensor solution. The ability of the platform to recalibrate based on surrounding environment makes it an adaptable, general purpose wearable device. The platform is able to provide real-time statistical analysis of different vapor and liquid footprints, including alcohol and can be calibrated to the needs of the user. This low powered platform has long lasting rechargeable battery and has a user interface that gives instant feedback of the data gathered to the individual user. It also contains the ability to connect to external devices, such as mobile devices or computers, for even further in depth analysis of the data gathered. All of these features are placed in a condensed and custom made printed circuit board that can be fitted in a wearable device such as a watch for a natural feel to the user.

*S. Bhansali is the Chair and Alcatel-Lucent professor and chair of electrical and computer engineering department, Florida International University, Miami, Florida 33174 USA (corresponding author, phone: 305-348-4439; e-mail: sbhansa@fiu.edu).

## II. Experimental

### A. Materials and Apparatus

Nafion perfluorinated 424 reinforced with poly-tetra-fluoro-ethylene (PTFE) fibers (thickness 0.03 cm) was purchased from Sigma-Aldrich and used as a proton exchange membrane (PEM). Nickel coated micro-perforated stainless steel with the thickness of 0.02 cm and pore size of 180 μm was used as the electrode material to develop a fuel cell sensor (Advanced Materials Engineering Research Institute, Florida International University). Nickel chloride anhydrous, nickel sulphamate, boric acid, 95% sulfuric acid, $H_2SO_4$ and 37% hydrochloric acid, HCl were purchased from Sigma-Aldrich for nickel electroplating. Lead and nickel sheet were purchased from McMaster-Carr and were used as electrodes for nickel electroplating process. Acetone and ethanol (95.27%) were purchased from Fisher scientific Inc. All other used chemicals were of analytical grade. The preparation of aqueous solutions was done with de-ionized (DI) water.

For miniaturized potentiostat construction, analog front end (AFE) potentiostat (LMP91000), 16-bit ultra-low power microcontroller MSP430F5529LP, and Bluetooth (RN-42) were purchased from Texas Instruments. For the power management system, the voltage regulator LP2591 from TI and the charge controller MCP72831 from Microchip were used in the circuitry. Additionally, 12 bit digital-to-analog converter with integrated EEPROM and an I2C compatible serial interface from microchip were also employed in the circuit. Moreover, various types of resistors, capacitors and inductors were also used to construct the electronic circuitry.

Open circuit potential (OCP) and amperometric studies were performed in analytical systems model potentiostat CHI 1230B containing MC470 purchased from CH instruments Inc. Autolab PGSTAT30 (potentiostat/galvanostat) was used

978-1-5090-3087-3/16/$31.00 ©2016 IEEE

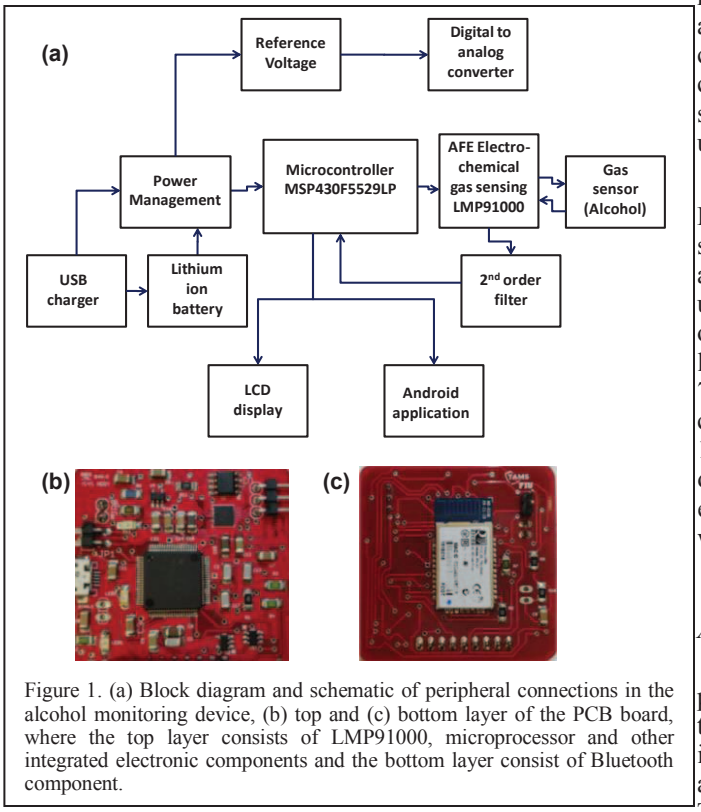


Figure 1. (a) Block diagram and schematic of peripheral connections in the alcohol monitoring device, (b) top and (c) bottom layer of the PCB board, where the top layer consists of LMP91000, microprocessor and other integrated electronic components and the bottom layer consist of Bluetooth component.

for the electroplating of nickel on the micro-perforated stainless steel [13]. The standard concentrations of ethanol were measured using MICRO5 PID sensor purchased from BW Technologies. The working and counter electrodes in the fuel cell sensor were nickel coated micro-perforated stainless steel sheets and the reference electrode was a non-conventional standardized electrode. Ethanol vapor was generated by bubbling a constant flow of air through a 15.8M ethanol solution. During measurements, the generated ethanol vapor was passed through the chamber (volume of ~0.7 $cm^3$) containing standard PID sensor or the developed fuel cell sensor. The chamber was designed in such a way that the counter electrode was exposed to the atmosphere. The chamber was built by a 3D printer (model: Replicator 2) which was purchased from Makerbot.

### *B. Potentiostat Platform and Fuel Cell Sensor Construction*

The developed fuel cell sensor was interfaced with the LMP91000 analog front end (AFE) on a wearable platform. The working, reference, and counter electrodes of the sensor were connected to the corresponding pins of the AFE. The AFE was linked to the microcontroller via inter-integrated circuit (I2C) interface. The Bluetooth module was connected via universal asynchronous receiver/transmitter (UART) peripheral of the MSP430. The liquid crystal display (LCD) used the serial peripheral interface (SPI). The connections and their functions are discussed in the results and discussion. The peripheral connection is depicted in the block diagram as shown in Figure 1a.

The printed circuit board (PCB) was manufactured in two layers using a 1.6 mm thick FR-4 substrate with 28.35 g copper and an overall dimension of 6.45 $cm^2$. The top layer consists of all the electronic components including the microcontroller, AFE, power management system, and associated circuitry as shown in Figure 1b. The bottom layer consists of the Bluetooth solely (Figure 1c). The PCB components were assembled manually using the rework soldering station air-gun 852D. Solder work was performed utilizing a 3mm ESD tip at a temperature of 450˚ C.

The fuel cell sensor was constructed by sandwiching PEM between micro-perforated sheet electrodes. Before sandwiching, the pieces were ultrasonicated for 3 to 5 min in a detergent and subsequently cleaned with DI water, then ultrasonicated in acetone for 3-5 minutes to remove any organic residues. Sandwiching was achieved by pressing the layers with the hydraulic hot press (model 2100 from PHI) at 75˚ C and 2500 psi for 10 mins. The area of the PEM, counter, working, and reference electrodes were 1.5x1, 1.5x1, 1.5x0.8, and 1.5x0.2 $cm^2$, respectively. The sensor is designed in such a way that the counter and reference electrodes were pasted onto the facet of the PTFE and the working electrode on the Nafion membrane.

## III. Results and Discussions

### *A. Electrochemical Mechanism of Ethanol Fuel Cell Sensor*

The operation of any PEM fuel cell sensor depends primarily on (i) the redox oxidation and reduction reaction at the anode and cathode surface, (ii) the PEM's hydration and its ability to transport protons from the anode to the cathode, and (iii) the catalyst's ability to enhance the redox reaction. The anodic and cathodic reactions of the ethanol fuel cell can be represented by equations (1), (2). The overall fuel cell reaction can be represented by equation (3) [14,15].

$$C_2H_5OH + 3H_2O \rightarrow 12H^+ + 12e^- + 2CO_2 \quad (1)$$

$$3O_2 + 12H^+ + 12e^- \rightarrow 6H_2O \quad (2)$$

$$C_2H_5OH + 3O_2 \rightarrow 2CO_2 + 3H_2O \quad (3)$$

During this redox reaction, protons are exchanged from the anode to the cathode through the PEM, and the electrons flow through the internal circuit. The potential difference between the anode and cathode was measured by the OCP technique (time vs. voltage). The measurements were taken over a period of 1,000 s in a closed chamber containing the fuel cell sensor, then the ethanol was introduced into the system after the sensor reached and maintained a steady state potential. Even though the steady state potential was attained by the sensor within t=5s, t=100s was chosen to introduce the ethanol in order to understand the minute changes of the OCP in a controlled environment. The response time of the sensor in the OCP technique is about 2s. In this study, Ni was chosen as the catalyst for both anode and cathode reactions because it enhances both oxygen reduction and ethanol oxidation reaction rates [14,15]. It is known that the rate and amount of proton exchange depends on the water content of the PEM [16,17]. To minimize the effect of humidity on $H^+$ ion transport in PEM, each sensor was treated in humidity for 30 min under room temperature before experiments. However, the experimental results revealed that there was a -0.2 V deviation in OCP once a water droplet was introduced on the anode. This deviation varies with the percent change in humidity. In the same experiments, the OCP of the fuel cell sensor in the presence of 95.6% ethanol under the same

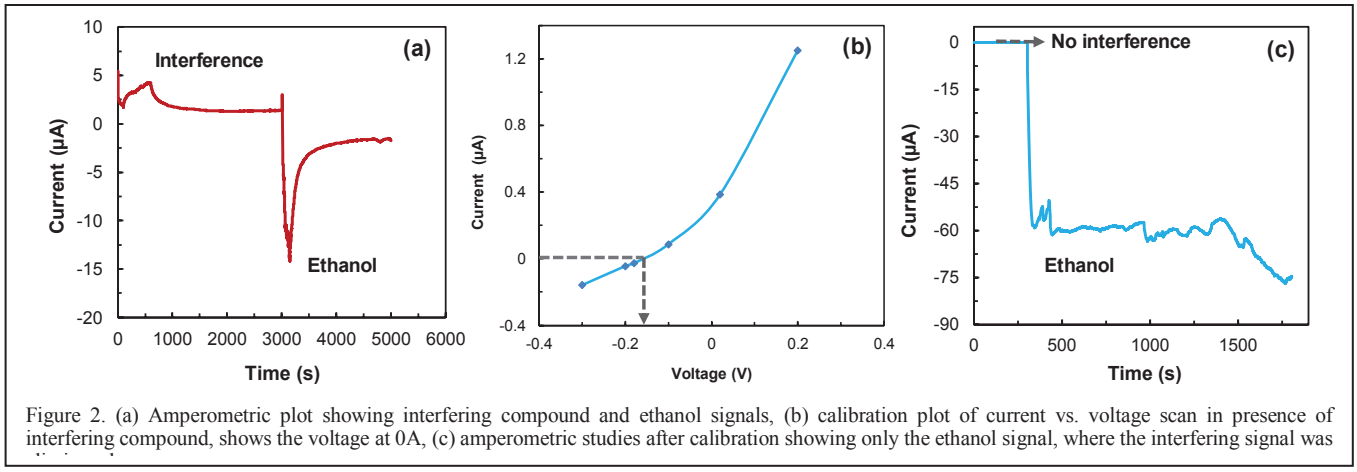


Figure 2. (a) Amperometric plot showing interfering compound and ethanol signals, (b) calibration plot of current vs. voltage scan in presence of interfering compound, shows the voltage at 0A, (c) amperometric studies after calibration showing only the ethanol signal, where the interfering signal was

humidity conditions was measured to be 0.07 V. In the experiments with low humidity (<60%) ±0.03 V deviation was observed in ethanol signal.

In real-world conditions the amount of humidity varies inconsistently. The exposure of various percentage of humidity on the fuel cell sensor reveals that the reference value of the OCP signal oscillates. Therefore, deriving a relationship between humidity and the OCP signal generation for calibration is not possible based on empirical results. Similarly, ethanol measurements in the presence of other organic volatile compounds also affect the sensors calibration. Hence, quantifying ethanol based on the OCP technique alone would be inaccurate, even though significant

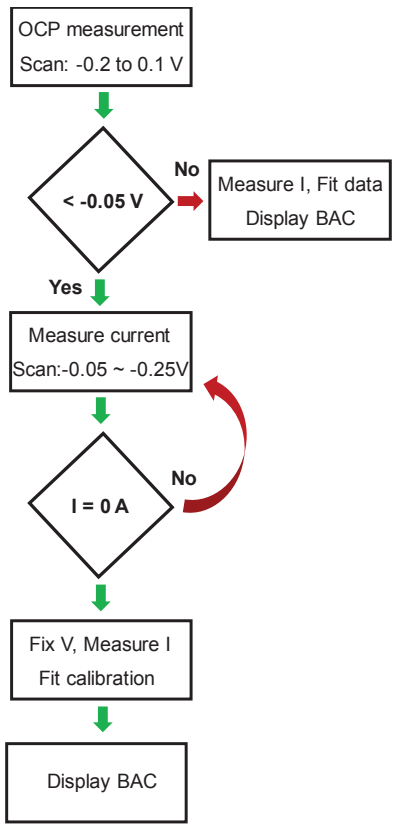


Figure 3. Flow chart representing steps involved in selective ethanol detection.

signals were measured for ethanol. The OCP results also revealed that the voltage of the fuel cell in presence of ethanol is 0.4 V more positive than the signal due to water/humidity. This signal variation between ethanol and the interfering compound provided an opportunity to design a method to eliminate interference. Similar to humidity, any organic volatile compounds capable of oxidizing on the anode has its own OCP signature.

### *B. A Method to Eliminate the Interfering Signal*

Selectivity is the biggest challenge in the successful construction of a fuel cell sensor. In a diffusion controlled process, the OCP, due to any given reaction, is independent of its concertation. However, in the case of low concentration and low volume measurements, the rate of the reaction, rate of diffusion, and rate of evaporation are the limiting parameters. The sensor accuracy will be low if the concentration of the interfering compound is much higher than the ethanol, or if the concentration of ethanol is much lower than ambient volatile compounds. As discussed above, the formal potential of each compound will also vary along with their OCP. To improve accuracy, a multimodal method containing both OCP and amperometric techniques has been employed for subsequent measurements.

It is known that during the redox reaction the current flows between the electrodes, and this faradaic current can be measured using amperometric method. The current generated in the amperometric experiments depends on (i) formal potential of the reactions, (ii) applied potential across the electrodes, and (iii) rate of the redox reaction. For example, the amperometric measurement of liquid ethanol at a fixed potential (-0.05 V) in presence of interfering compound (water droplet) given in Figure 2a reveals that there is a response for not only ethanol but the interfering compound as well. The same figure shows that if the applied potential is lower than the OCP of any given compound, it has negative current response, similarly the opposite has positive current response, where the OCP of ethanol and sensor in water is 0.05 and -0.15 V respectively. Depends on the difference (ΔV) between OCP and the applied potential the output current varies. This shows that the rate of faradaic reactions on the electrode surface can be manipulated using external voltage. As a first step towards eliminating interference signals, signal due to humidity was taken as an example for the following studies. Same method can be applied for

eliminating the signals of all other organic volatile compounds. However, the developed method is only applicable for binary chemical compounds and not for multiple interfering compounds.

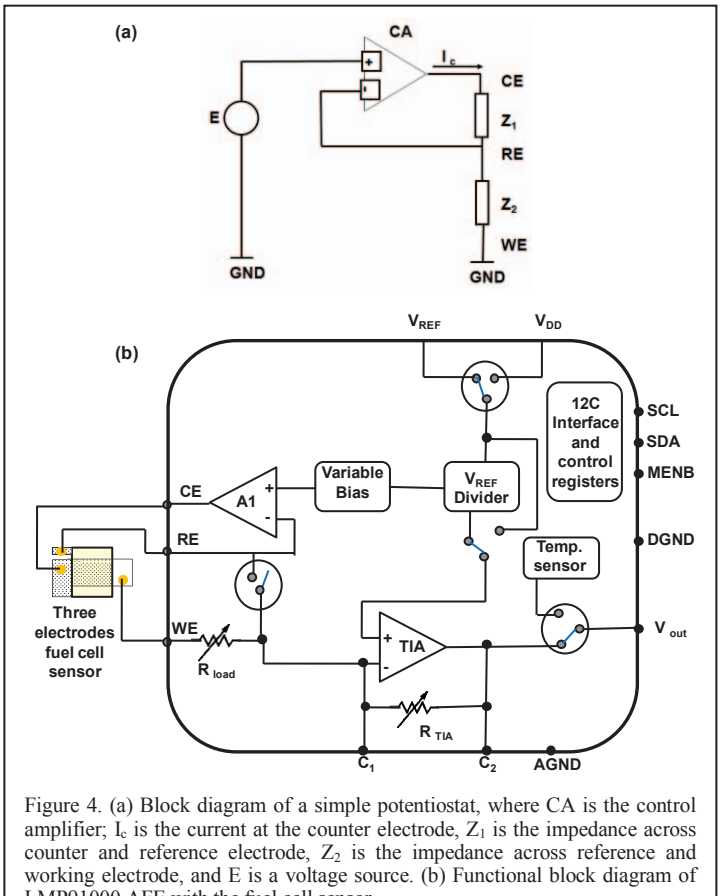


Figure 4. (a) Block diagram of a simple potentiostat, where CA is the control amplifier; $I_c$ is the current at the counter electrode, $Z_1$ is the impedance across counter and reference electrode, $Z_2$ is the impedance across reference and working electrode, and E is a voltage source. (b) Functional block diagram of LMP91000 AFE with the fuel cell sensor.

The selectivity of ethanol in presence of any one of the interfering compound has been achieved by the following method. The steps involve, (i) identifying the OCP of the fuel cell sensor in the presence of the interfering compound, and (ii) applying the obtained OCP value across the anode and cathode and measuring the current flow. In this process the current signal due to interfering compound has been eliminated and the current flow due to ethanol oxidation for that particular potential was recorded. The experiments with humidity (60 to 100%) showed that the OCP of the fuel cell sensor varies from -0.05 to -0.25V. By keeping the electrode potential exactly at the full cell potential ($E_{cell}$) at any given humidity level (in the absence of ethanol), the current flow due to humidity has been eliminated.

The identification of the $E_{cell}$ in presence of water droplet was carried out by a series of amperometric studies, where various potentials were applied across the electrodes and the current was measured (Figure 2b). From the applied potential vs. current plot the exact $E_{cell}$ at which the current has 0A can be identified for that particular condition. Even though the steady state OCP measurements can be used to measure this $E_{cell}$ value, the amperometric method was used to find the $E_{cell}$ to significantly improve the accuracy. In real-time calibrations, attaining OCP steady state varies depending on the environment and the need for prolonged scans. The amperometric results after calibration (Figure 2c) shows the ethanol signal only, and the signal interference due to water has been eliminated.

### C. *Algorithm for the Sensor Auto-Calibration*

Based on the experimental observations in the previous section, a flow chart (Figure 3) was derived for construction of a wearable potentiostat with auto-calibration ability and selectivity to ethanol in high humid conditions. The same method can be used for any interfering compound with the OCP higher or lower than ethanol. The nullification of current signal produced by interfering compound was achieved by two following functions.

*function 1:* auto-calibrate fuel cell sensor in certain intervals (intervals changes depend on the steady state response of the nickel catalyst).

*function 2:* measurement of ethanol using amperometric measurement.

The calibration (1st function) is necessary to know the interfering signal level and nullify the interference signal in the second function. The 1st function involves OCP and amperometric measurements, the 2nd function involves amperometric measurements. In the 1st function if the value is lower than the threshold OCP value, it indicates no ethanol present and proceed to amperometric measurements. In this step $E_{cell}$ for 0A is identified by measuring current across the electrodes while scanning the potential. The obtained $E_{cell}$ value is stored in the device. This stored value will be the bias voltage for amperometric measurements in the 2nd function, where the current is measured and fitted against a pre-determined calibration curve. In the device memory, there will be multiple pre-determined calibration curves stored for each biasing voltage. Multiple pre-determined calibration curves were used because the current signal magnitude in the 2nd function depends on the biasing potential. The final step is to display BAC from the calibration curve fitting. This process will nullify the interfering signal in any given environment.

### D. *Configuration of the Analog Front End Alcohol Sensing Device*

A schematic of the potentiostat is given in Figure 4a. The arrangement of the circuit is that of a non-inverting operational amplifier. The voltage supplied by the source E, is closely followed by the voltage between the RE and WE terminals. $Z_1$ and $Z_2$ are the characteristic impedances of the fuel cell between the respective terminals. Any change in impedance due to ethanol coming in contact with the working electrode (WE) is reflected by the change in current $I_c$ (current at counter electrode), as show in figure. The impedance at the negative terminal of the amplifier is very high which makes the current flowing through the reference electrode negligible. This is important since any current flowing through the reference electrode would change its potential.

The LMP91000 used in this work is a miniaturized potentiostat from Texas Instruments that can be configured to perform different types of electro-analytical techniques. The

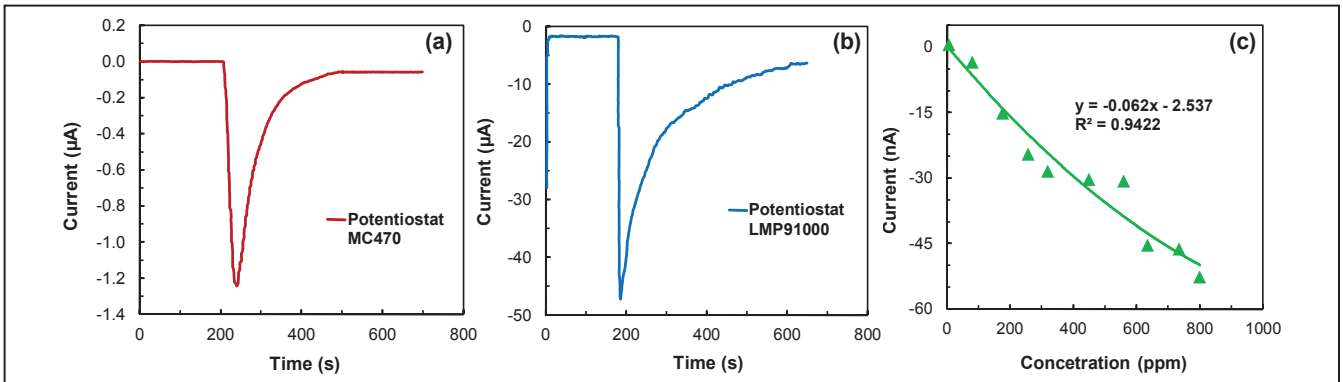


Figure 5. Amperometric data obtained in (a) commercial MC470 potentiostat and (b) LMP91000 potentiostat in presence of ethanol vapor and humidity (c) concentration vs. current plot showing the linear calibration curve for ethanol.

detection method used in the system was amperometric. Referring to figure 4b, amplifier A1 is the control amplifier that implements the potentiostat circuit. The variable bias block of the LMP is used to provide a user configured potential across positive and negative terminals of A1. This potential is held constant between the reference and working terminals by the potentiostat.

The TIA or transimpedance amplifier is a current to voltage converter. The transition from minimal current flow to voltage is made available by the TIA whose forward voltage gain is dependent upon on a feedback resistor $R_{tia}$. It can be connected either internally or externally to the feedback path of the TIA as depicted in the internal block diagram of the AFE LMP91000 in Figure 4b [18]. It converts the current flowing from counter electrode (CE) and WE to a proportional voltage. Its output is connected to Vout pin (this pin can be toggled to give output of the temperature sensor of the LMP) and the C2 pin.

The LMP was configured via the microcontroller to perform three electrode amperometry following the functional block diagram sketched in Figure 4b. The WE, reference electrode (RE) and CE of the sensor were connected to the corresponding pins of the LMP as shown in Figure 4b. The microcontroller connects to the LMP via the I2C interface, as depicted in Figure 1a and 6b. The serial clock line (SCL) and serial data bus (SDA) line on the I2C bus were connected to $3.3V_{dc}$ from the system power management unit with one external pull up resistor each. The schematic representation in Figure 4b was derived for the 3-lead amperometric cell in potentionstat configuration [18]. The output voltage available at the $V_{out}$ pin of the LMP91000 is then routed to the microcontroller general purpose input/output (GPIO), where it is conditioned by an internal analog-to-digital converter for interpretation. The trans-impedance amplifier gain is adjusted to provide a voltage proportional to cell current, it can be internally programmed via software for a range of $2.5k\Omega \leq R\_tia \leq 350k\Omega$ and externally configured as required.

The internal feedback resistor has been optimized for an optimal TIA amplifier gain using a value of $R_{TIA}$= 120kΩ, this provides a large enough signal gain to manipulate the data and provides enough headroom for voltage swings as a result of changes in alcohol concentration. The module enable (MENB) is tied to ground in order to signal a communication ready status to the microcontroller. In the case of multiple alcohol sensors, the MENB line of each AFE sensing device on the I2C bus can be toggled through to extract data from each sensor individually. The voltage reference ($V_{REF}$) to the analog front end sensing device was externally provided by the digital to analog converter (MCP4724) and was adjustable through software and can meet a wide range of supply voltages to the LMP91000 and to specify bias voltages with accuracy. The load resistor was set to its lowest internal resistance value of $R_{load}$=100Ω in order to draw maximum current from the sensor and subsequently become amplified by the TIA.

### *E. Microcontroller Operation and Alcohol Concentration Measurement Technique*

The microcontroller unit (MCU) (MSP430F5529LP from Texas Instruments) has been chosen due to its small LQFP-80 pin packaging size, low power mode (LPM) settings that allow power consumption down to 1.4 µA in LPM3, low operating voltage range of $1.8\,V_{DC} \leq V_{Batt} \leq 3.7\,V_{DC}$ and portability to other microprocessing units if so desired due to the simplicity of the C programming language. Features that made the MSP430F5529LP attractive for our application were its ability to store 128 kB of non-volatile flash memory and 8 kB of RAM, allowing the software to execute during power-on and reset events, and a 12-bit ADC that was used to measure the analog output of the LMP.

The MCU has the capability to communicate via SPI, UART, and I2C. The alcohol sensing platform uses I2C to communicate with the LMP91000 and MCP4724, UART to communicate with the RN-42 Bluetooth module and SPI to communicate with the monochrome LCD. The current and proposed configuration for the MCU is shown in Figure 1b. In this figure we can see the MCU can be programmed and debugged on-chip and on a minimally system invasive procedure simply by connecting two Spy-Bi-Wire emulator cables. The external circuitry shown in Figure 1b are bypass capacitors and ground connections required for proper MCU operation, this configuration has been derived from a device specific datasheet and user guide. The algorithm for interpreting sensor data has been derived from [19]; under this configuration two additional cables are routed from the LMP91000 *C1* and *C2* pins to the MSP430F5529LP GPIO pins. The data from *C1* and *C2* consists of the analog output voltage $V_{out}$ of the LMP91000 and the analog voltage present at the inverting input of the TIA, who is directly connected to the working electrode of the three-electrode sensor and is the

same voltage at the non-inverting input of the TIA, this was a fixed percentage of the $V_{REF}$ or divided reference voltage ($V_{REF_{DIV}}$), and is chosen dependent on current flow to the WE. Through this procedure it can be derived the current flowing at the working electrode of the three electrode system ($I_{WE}$) as follows $I_{WE}= (V_{out} - V_{REF_{DIV}})/R_{TIA}$ , once $V_{REF_{DIV}}$ has been established using the aforementioned procedure, $R_{TIA}$ was chosen depending on the sensitivity of the sensor given in parts-per-million (ppm) as previously discussed, the current of the sensor is then calibrated via software as a function of all described parameters.

### *F. MC470 and LMP91000*

To validate the device, data from the commercially available electrochemical device MC470 has been compared with the constructed LMP91000 device as shown in Figure 5a and b respectively. During these experiments, both the devices were placed in an identical setup with similar parameters as given in the experimental section. The concentration of ethanol vapor used for these experiments was 335000 ppm. The experiments were carried out for 700s, where the humidity was introduced after 50s and the ethanol was introduced after 200s. The biasing potential was kept constant at -0.2V for both the experiments. Both the results showed there were no interfering signal due to humidity, and has response to the ethanol (Figure 5a and b). Comparison of the results in the same figure shows that the LMP91000 device has 30 times higher current signal due to the presence of amplifier in the device.

The effect of ethanol vapor concentration on the fuel cell sensor was studied for sensor evaluation. In these experiments, there were ten different concentrations tested in the physiological range of transdermal ethanol (5 to 800 ppm). The optimized sensor operating parameters were 42% humidity at 25˚C. The concentration vs. current plot given in Figure 5c shows that the sensor response is linear from 5 to 800ppm with the sensitivity of 0.062 nA $ppm^{-1}$ with the lowest detection limit of 5ppm. These results prove that the device along with the sensor has the capability to measure even the lowest transdermal ethanol concentration (~200ppm).

## IV. CONCLUSION

A miniaturized alcohol monitoring system containing small scale fuel cell sensor with a compact potentiostat has been developed. The device includes data processing and transmission units with low power consumption which can also provide highly stable signal. The electrochemical studies provided a pathway to design a method to eliminate any interfering signal in a fuel cell sensor. An algorithm was developed to implement auto-calibration ability in the developed device to improve the selectivity towards ethanol. The method for eliminating signal due to humidity in this work demonstrated potential pathway for eliminating any organic volatile compound interfering signal. The modification of nickel plated electrode with the thin film catalyst could be a prospective development of the present work, where sensitivity and detection limit can be improved several fold.


## ACKNOWLEDGMENT

This work was supported by ASSIST NSF ERC and the NSF I-Corps Teams.


## REFERENCES


[1] O. Chestnov, "*Global status report on alcohol and health*," World Health Organization (WHO), pp. 1-25, 2014.

[2] R. Room, T. Babor, and J. Rehm, "Alcohol and public health," *The Lancet*, vol. 365, pp. 519-530, Feb. 2005.

[3] R. A. Goodman, J. A. Mercy, F. Loya, M. L. Rosenberg, J. C. Smith, N.H. Allen, L. Vargas, and R. Kolts, "Alcohol Use and Interpersonal Violence: Alcohol Detected in Homicide Victims," *AJPH*, vol. 76, pp. 144-149, Feb. 1986.

[4] Dept. of Transportation (US), *National Highway Traffic Safety Administration (NHTSA)*, "Traffic Safety Facts 2013 Data: Alcohol-Impaired Driving," Washington (DC): NHTSA; 2014.

[5] C. L. Sanford and B. A. Mantooth, "Determination of ethanol in alcohol samples using a modular Raman spectrometer," *J Chem Educ*, vol. 78, pp. 1221-1224, Sep. 2001.

[6] A. A. Shabaneh, S. H. Girei, P. T. Arasu, W. B. W. A. Rahman, A. A. A. Bakar, A. Z. Sadek, H. N. Lim, N. M. Huang and M. H. Yaaco, "Reflectance response of tapered optical fiber coated with graphene oxide nanostructured thin film for aqueous ethanol sensing," *Optics Comm*., vol. 331, pp. 320-324, Nov. 2014.

[7] T. K. An, H. -J. Yun, R. Narote, R. Kim, S. U. Lee, Y. Kim, S. Nam, H. Cha, Y. J. Jeong, K. Kim, S. Cho, S. -K. Kwon, Y. -H. Kim and C. E. Park, "Synthesis and characterization of an ester-terminated organic semiconductor for ethanol vapor detection," *Org Electronics*, vol. 15, pp. 2277-2284, Oct. 2014.

[8] M. -R. Yu, G. Suyambrakasam, R. -J. Wu and M. Chavali, "Performance evaluation of ZnO–CuO hetero junction solid state room temperature ethanol sensor," *Mat Res Bulletin*, vol. 47, pp. 1713-1718, Jul. 2012.

[9] R. A. Kadir, R. A. Rani, A. S. Zoolfakar, J. Z. Ou, M. Shafiei, W. Wlodarski and K. Kalantar-zadeh, "Nb2O5 Schottky based ethanol vapour sensors: Effect of metallic catalysts," *Sens Act B: Chem*., vol. 202, pp. 74-82, Oct. 2014.

[10] H.- J. Kim and J. -H. Lee, "Highly sensitive and selective gas sensors using p-type oxide semiconductors: overview," *Sens Act B: Chem*., vol. 192, pp. 607-627, Mar. 2014.

[11] J. T. Sakai, S. K. Mikulich-Gilbertson, R. J. Long and T. J. Crowley, "Validity of transdermal alcohol monitoring: Fixed and self-regulated dosing," *Alcoholism: Clinical and experimental research*, vol. 30, pp. 26-33, Jan. 2006.

[12] A. S. McKnight, J. C. Fell, and A. Auld-Owens, "*Transdermal Alcohol Monitoring: Case Studies*," U.S. Department of Transportation, Aug. 2012.

[13] W. B. Harding, "*Testing of Metallic and Inorganic Coatings*", ASTM International, pp.327-328, 1987.

[14] J. Friedl, U. Stimming, "Model catalyst studies on hydrogen and ethanol oxidation for fuel cells," *Electrochim. Acta*, vol. 101, pp. 41-58, Jan. 2013.

[15] E. Antolini, "Catalysts for direct ethanol fuel cells," *J. Power Sources*, vol. 170 pp. 1-12, Apr. 2007.

[16] H. Junming, X. Liangfei, L. Jianqiu, M. Ouyang, C. Siliang, F. Chuan, Water management in a self-humidifying PEM fuel cell system by exhaust gas recirculation, *ITEC Asia-Pacific, 2014 IEEE Conference and Expo*, pp.1-6, Aug. 2014.

[17] C. Hartnig and C. Roth, "*Polymer electrolyte membrane and direct methanol fuel cell technology*," Elsevier, pp.291-297, Feb. 2012.

[18] Texas Instruments, "*LMP91000 Sensor AFE System: Configurable AFE Potentiostat for Low-Power ChemicalSensing Applications,*" LMP91000 datasheet, Jan. 2011. (Revised Dec. 2014).

[19] Ž. Mihajlović, V. Milosavljević, V. Rajs, F. Milivojčević, M. Živanov, "Miniature low cost electrochemical sensor module for measurement of gas concentration," TELFOR*, 22nd*. IEEE, pp. 702-705, Nov. 2014.